Defense Technical Information Center
Compilation Part Notice

ADP011197

TITLE: Exit Wave Reconstructions of Surfaces and Interfaces Using Through Focus Series of HREM Images

DISTRIBUTION: Approved for public release, distribution unlimited

This paper is part of the following report:

TITLE: Internal Workshop on Interfacially Controlled Functional Materials: Electrical and Chemical Properties Held in Schloss Ringberg, Germany on March 8-13, 1998

To order the complete compilation report, use: ADA397655

The component part is provided here to allow users access to individually authored sections of proceedings, annals, symposia, etc. However, the component should be considered within the context of the overall compilation report and not as a stand-alone technical report.

The following component part numbers comprise the compilation report:
ADP011194 thru ADP011211

Exit wave reconstructions of surfaces and interfaces using through focus series of HREM images

H.W. Zandbergen[a,*], D. van Dyck[b]

[a]*National Centre for HREM, Laboratory of Materials Science, Delft University of Technology, Rotterdamseweg 137, 2628 AL Delft,
The Netherlands*
[b]*EMAT, University of Antwerp (RUCA), Groenenborgerlaan 171, B2020 Antwerp, Belgium*

Abstract

The through focus exit wave reconstruction technique uses a series of high resolution electron microscopy (HREM) images to reconstruct the complex electron wavefunction at the exit plane of the specimen. The main advantage of this technique compared to conventional HREM is better interpretable images due to the deblurring of the information. This is in particular valid for surfaces and interfaces, as is shown by examples of exit waves of a (001) surface of NiO, a single slab of $(Mo,Co)S_2$ on γ-Al_2O_3 and the sapphire/CeO_2 interface. © 2000 Elsevier Science B.V. All rights reserved.

Keywords: High resolution electron microscopy; Surfaces; Interfaces; Exit wave reconstructions

1. Introduction

Knowledge of the atomic arrangements of surfaces and interfaces is of vital importance for the understanding of the properties. With the increasing need of the accurate determination of the atomic arrangements at non-periodic structures in materials design and control of microstructures and nanostructures, techniques that allow quantitative structural information at the sub-angstrom level will be indispensable. Compared to other techniques used to obtain structural information of materials, high resolution electron microscopy (HREM) has the great advantage that it yields local information about the atomic arrangements, projected along the direction of electron incidence at a resolution comparable to the interatomic distances. By combining the information obtained from different projections one can in principle obtain three-dimensional structural information.

Several groups [1–5] have used HREM to determine the atomic arrangements at selected grain boundaries with a high precision. Yan et al. [6] have shown that it is even possible to determine the composition of individual atom columns, using electron energy loss spectroscopy. Still the fraction of grain boundaries that can be studied by conventional HREM is limited. Recent developments in the processing of HREM images make it possible to reconstruct the electron wavefunction at the exit of

*Corresponding author. Tel.: +31-15-278-2266; fax: +31-15-278-6730.

E-mail address: h.w.zandbergen@tnw.tudelft.nl (H.W. Zandbergen)

the object. At present two methods are used in a routinely manner for exit waves reconstructions: through-focus electron holography and off-axis electron holography [7–9]. A major advantage of the reconstructed exit wave is that it allows a more straightforward quantitative interpretation than HREM images, in particular for non-period features like grain boundaries.

The recent papers in this journal, for which HREM was applied as a major experimental tool, can roughly be divided into three groups. The first group concerns the investigation of substitutions and the presence of extra atoms and vacancies [10–12], whereby one is mainly interested in the (super)structure. In the case only small crystals are available and one is interested in the average structure, the best tool is quantitative electron diffraction [13,14]. The second group is the study of the morphology and the microstructure [15–17]. The third and most important group is the investigation of grain boundaries (atomic structure, presence of second phases, local composition) [17,18]. In the present paper we will concentrate on the last group, HREM on grain boundaries and surfaces, because in this field the use of exit wave reconstruction has the most advantages.

In the HREM investigation of grain boundaries three aspects are very important restrictions: the shape and orientation of the grain boundary, the crystal lattices of the adjacent crystals and the resolution of the electron microscope.

The shape and orientation of the grain boundary is important, because HREM provides in first approximation projections of the structure, such that only lateral information and no depth information is available. This implies that the information of a grain boundary that is not parallel to the electron beam will be smeared out. Concerning the determination of rough shapes, a lot of development has been done in the last few years on the determination of the shape of biological particles by means of electron tomography [19,20]. The present state of the art is that a 3D resolution of about 1 nm can be obtained. For this a tilt series from $-70°$ to $+70°$ with increments of $2°$ are typically used. The 3D reconstruction of these biological specimens is based on contrast changes due to the overlap of scattering material in projection. In the study of inorganic solid state materials a 1-nm resolution is insufficient and also

more difficult to obtain. The 1-nm resolution is insufficient because one will be interested in the atomic arrangements at the grain boundary (e.g. even an amorphous grain boundary layer of 0.5 nm can strongly influence the properties). The 3D reconstruction of grain boundaries is more difficult when these materials consist of (small) crystals. Crystallinity results in extra contrast, which depends very strongly on the orientation. In orientations where the crystal is in a low-index[1] orientation, it scatters the electrons much stronger than in a high-index orientation. This cancels the one-to-one correspondence between contrast and the projected average scattering potential.

A crystalline specimen allows one to obtain a structure image. In this case one has to orient the crystal such that the projection of the structure along the electron beam results in image features that can be resolved given the resolution of the electron microscope. This implies that the imaging can only be done with the electron beam along a small selection of crystal directions. Obviously, the better the resolution of the electron microscope the more directions can be used.

If the crystal is perfectly aligned, the atoms can be considered as aligned in columns. In this case a column scattering potential [21], as schematically shown in Fig. 1, can replace the scattering potential of the atoms. The column scattering potential depends on the weight of the atoms and their distance along the column. If the crystal is tilted such that the column is not exactly along the electron beam (mistilt less than $1°$) this column approach is still valid [22].

Summing up the requirements for obtaining HREM images of grain boundaries that can be interpreted in a straightforward way: (i) the grain boundary is straight, (ii) the grain boundary is parallel to the electron beam, (iii) one of the grains and preferable both are in such an orientation, that lattice imaging is possible. Obviously most of these requirements become the more stringent the thicker the specimen. On the other side, a too thin specimen might not reflect the initial structure of the grain boundary due to changes induced by the thinning of

---

[1]A low index orientation is an orientation [*hkl*] that has a low sum $h + k + l$.
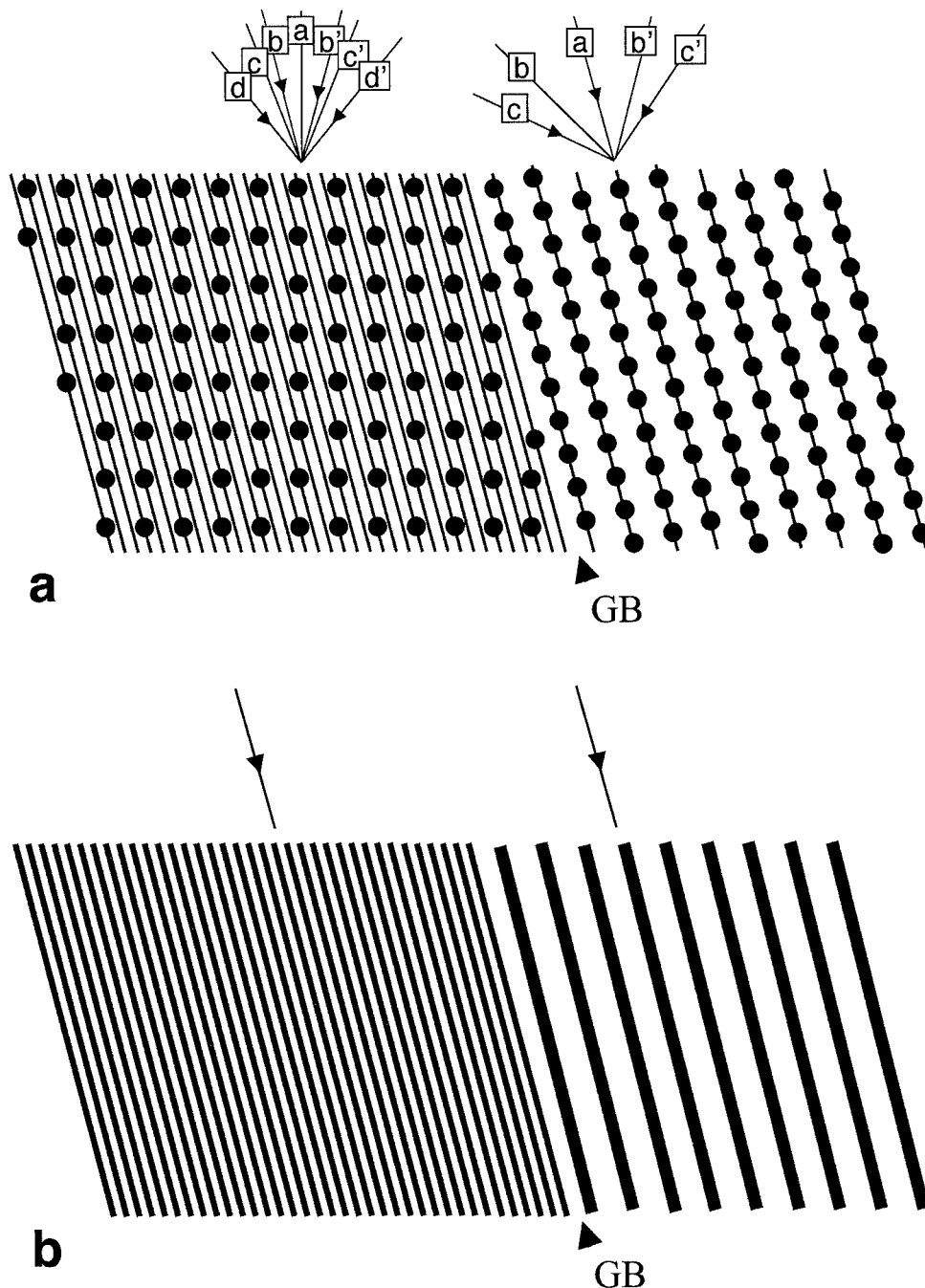
Fig. 1. (a) Schematic representation of an atomic arrangement around a grain boundary. It is supposed that lattice imaging is only possible along the directions a, b, c and d. The crystallographic arrangement of the grains is such that the direction b in the left grain is parallel to the direction a of the right grain, and the grain boundary is parallel to the a direction of the grain on the right. Because of that favourable orientation relation structure images of both grains are obtainable and the image of the grain boundary is as sharp as possible. For this orientation columns can replace the rows of atoms, each with its own scattering potential depending of the weight of its atoms and their spacing. The further the orientation deviates from the directions a, b, c and d, the poorer the contrast of the HREM images, which trend is faster for thicker specimens. Thus a very thin specimen will still allow an appreciable misorientation (several degrees).

the specimen or lattice relaxations due to the very limited thickness of the specimen. The interaction between electrons and matter is very large (about 10^4 times larger than for X-rays), such that very small specimen thicknesses can be investigated. The specimen thickness required for a good image contrast ranges from 1 to 10 nm depending on the scattering potential. This implies that the requirements that the electron beam is parallel to the grain boundary and parallel to atom columns are not very stringent. Obviously, the better the resolution of the microscope, the more directions one can get structural images from. In particular for the study of grain boundaries this increase in suitable directions is important.[2]

Compared to the imaging of the atomic arrangement at a grain boundary, the imaging of the atomic arrangement of a surface is much easier. In the first place the requirement that the second grain is also in an orientation allowing structure imaging does not have to be fulfilled. Secondly no information from the second grain, due to delocalisation of information, is complicating the interpretation of the image of the surface. In most cases the crystallographic planes occurring at grain boundaries are also the most stable surface planes, because such surfaces and interfaces tend will have a relatively low energy. Thus a surface can serve very well as a model material to investigate the atomic arrangements.

In this paper we want to illustrate the use of through-focus exit wave reconstructions, in particular on grain boundaries. To illustrate the differences in delocalisation of information between reconstructed exit waves and HREM images, we show some simple examples rather than giving examples of quantitative comparisons. Surfaces are used to illustrate the problems arising with the imaging of grain boundaries, because they can serve as simplifications of grain boundaries. After a short introduction to the resolution of the electron microscope and the delocalisation of information due to the imperfection of the microscope, three examples of reconstructed exit waves are discussed.

1.1. The resolution of the electron microscope

Concerning the resolution of a HREM, one has to distinguish between point resolution (or structural resolution) as the finest detail that can be interpreted directly in terms of the structure, and the information limit which is the finest detail that can be resolved by the instrument, irrespective of a possible interpretation. The electron microscope in the phase contrast mode at optimum focus (Scherzer focus) directly reveals the projected potential, i.e. the structure, of the object, provided the object is very thin and the atom columns are sufficiently separated. All spatial frequencies g with a nearly constant phase shift are transferred from object to image (see Fig. 2). Hence the point resolution, ρ_S, can be obtained from the first zero of the transfer function. The information
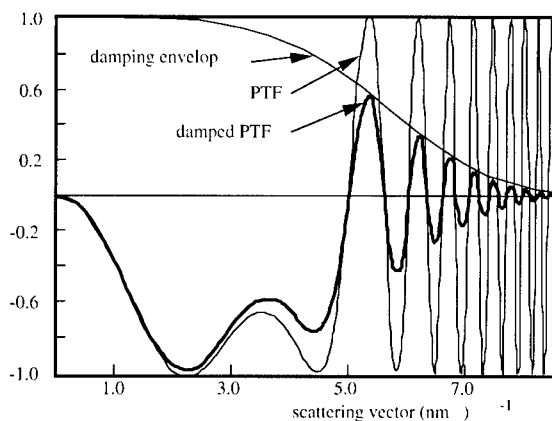

Fig. 2. Transfer function (imaginary part, and thus for the phase) for 300 kV with a C_S of 1.3 mm and a defocus of -63 nm (which is close to Scherzer focus). The damping corresponds to a defocus spread of 6 nm and a divergence of 0.1 mrad. The point resolution$=0.2$ nm and the information is 0.14 nm assuming that the contrast should be at least 10%.

---

[2] Assuming that a HREM allows a double tilt of $\pm 30°$, one out of three grain boundary can be aligned along the electron beam. Assume next that by rotation of the specimen about the interface normal with a range of 40°, one orientation can be reached allowing structure imaging for the first or the second adjacent grain. Then the chance of being able to have a grain boundary being parallel to the electron beam with the first grain only (the situation for a surface) is still one out of three. Assuming random orientation of the grains and that the maximum misorientation is 2°, the chance that an orientation can be found in which both grains are in a both grains in an orientation allowing structure imaging is 1 over 30. A doubling of the number of orientations allowing structure imaging increases this chance to 2 over 15.

beyond ρ_S is redistributed over a larger image area (delocalisation of information). In particular the high frequency information can be delocalised over several nanometers even for a good electron microscope and optimal imaging conditions. The information limit corresponds to the maximal diffracted beam angle that is still transmitted with appreciable signal-to-noise ratio. Since the information limit is mostly better than the point resolution, a promising way of increasing the resolution is by restoring the information that is present between ρ_S and ρ_I and which obviously has the wrong phase. This information has to be unscrambled for which purpose exit wave reconstruction has been developed. In that case ρ_I will determine the final resolution.

Recently two exit wave reconstruction methods to unscramble the delocalised information have been developed: through-focus electron holography and off-axis electron holography [7]. The exit wave reconstruction (unscrambling of the information) is done in two steps. First, the wavefunction in the image plane is reconstructed. Since by recording the image only the amplitude information is collected, one has to use a method to determine also the missing phase information. The phase in HREM images can be determined by holographic methods of which two approaches exist: off-axis holography [8] and focus variation [9]. For both techniques one needs a very high-resolution camera (CCD), a powerful image processor, and a field emission source to provide the necessary spatial coherence. In off-axis holography [8], the beam is split by an electrostatic biprism into a reference beam and a beam that traverses the object. Interference of both beams in the image plane then yields fringes, the positions of which yield the phase information. In the focus variation method, the focus is used as a controllable parameter so as to yield a through focus series from which both amplitude and phase information can be extracted [23–27]. Images are captured at very close focus values so as to collect all information in a three-dimensional space, composed of the intensities of the image $R(x,y)$ and the defocus. Schiske [23], Kirkland [24] and Saxton [25] have already suggested such methods. An alternative to the use of exit wave reconstructions is to improve the point resolution of the electron microscope. A 0.1-nm point resolution is already obtainable with

high-voltage high-resolution electron microscopes [28,29]. Such microscopes have as disadvantage their price and an increased chance of irradiation damage.

In the exit waver reconstruction, after determining the image wave one has to reconstruct the exit wave of the object. For this the microscope parameters have to be known very precisely. This forces the microscopist to perform the experiments with care and to decide beforehand which information he wants to achieve, such that the experiments are optimised to obtain this information. In the case one aims at the highest resolution, the best focus range is around Lichte focus (about three times Scherzer focus) for which the damping of the high frequency information is smallest.

Coene et al. [9] have developed a procedure to refine the exit wave by iteration comparing the simulated images for the whole through focus series. The best-matching criterion for this purpose is the maximum-likelihood criterion. In this way all information, both linear and non-linear, that is present in the images is fully exploited, so that the highest precision is achieved.

2. Experimental

Electron transparent areas of the various specimens were obtained by crushing (NiO and $(Mo,Co)S_2$ on γ-Al_2O_3) or by ion milling (sapphire/CeO_2 interface). The crushing was done under ethanol, after which a suspension was dripped onto a Cu grid with a carbon-coated holey film. The ion milling was done with the thin film side facing away from the ion gun with a final ion-polishing step using an acceleration voltage of 3 kV, a gun current of 0.3 mA, and an angle of 8°. Electron microscopy was performed with a Philips CM30ST electron microscope with a field emission gun operated at 300 kV and a Link EDX element analysis system. The information limit of this microscope is 0.14 nm. The high-resolution images were recorded with a 1024×1024 pixel Photometrix CCD camera with a dynamic range of 12 bits. For the through focus exit wave reconstructions (TF-EWR), a series of 15–20 HREM images was recorded with focus increments of 5.2 nm.

The choice of representation of the exit wave is to

a large extent arbitrary. One can either display a positive phase shift deviating from $2n\pi$ of the phase of an area having no atoms (e.g. vacuum) as black or white. Similarly a decrease in the amplitude can be displayed in two ways. In this paper the amplitude decrease and the positive phase shift in thin areas are displayed by a darkening. Thus for small thicknesses the heavy scattering atoms appear as dark dots in the amplitude as well as in the phase image, allowing easy comparison of these two images.

In order to determine the structure of a surface or interface by transmission electron microscopy one has to view parallel to the surface (profile imaging) or the interface as is shown in Fig. 3. Additional requirements are that one has to look in a direction along which the atoms are aligned in columns that are sufficiently separated and the specimen has to be very thin e.g. 20 nm or less.

2.1. Example 1: image calculations of a [100] surface of NiO imaged in profile

The complexity in the structure determination from conventional HREM images as compared to exit waves is demonstrated in Fig. 4. This figure shows calculated exit waves and calculated conventional HREM images for a range of defocus values of the (001) surface of NiO viewed along the [110] direction for two thicknesses, e.g. 1 and 5 nm. In the model used for this calculation all atoms have a Debye–Waller factor of 125 pm^2 except for the Ni atoms at the (001) surface, which have a Debye Waller factor of 375 pm^2. This Ni atom can be clearly distinguished in the amplitude of the exit wave, since it is much less dark. In the HREM images this different Ni atom is, however, not observable. In fact, these images would be almost the
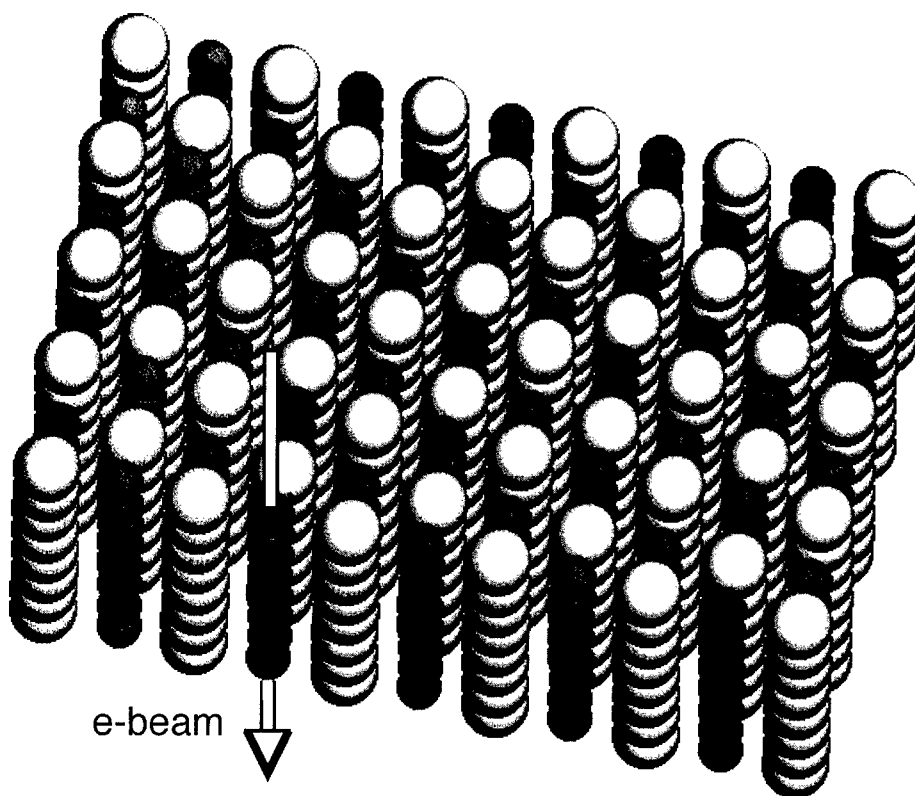

Fig. 3. Schematic representation of profile imaging. The arrow indicates the direction of the electron beam.
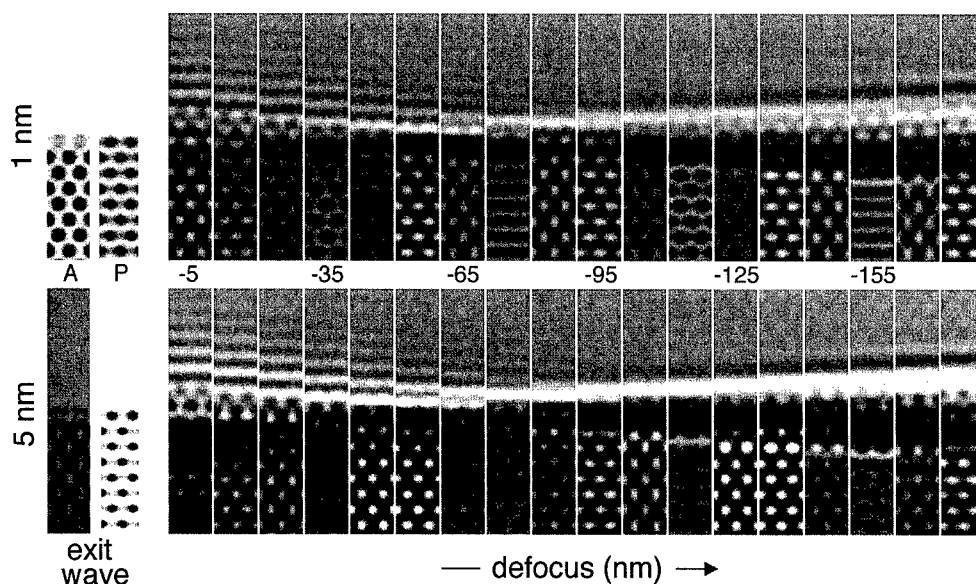
Fig. 4. Calculated images for a (001) NiO surface in profile imaging, using $C_s = 1.3$ mm, a defocus spread of 6 nm, a divergence of 0.1 mrad and a mechanical vibration of 0.05 nm.

same, if this Ni would have also a Debye–Waller factor of 125 pm^2.

One can see that in the HREM images the information of the surface is delocalised. The extend of this delocalisation depends on the defocus. The information of the 'single crystalline' part is of course also delocalised, but this is not visible due to the periodicity of this area. In this figure the smallest delocalisation seems to occur at a defocus of about -70 nm. However, this minimum delocalisation depends on the scattering angle, the wavelength and the spherical aberration of the objective lens. For a spherical aberration of 1.35 mm and a defocus of about -70 nm, a minimum delocalisation is obtained for a reflection g of about 5 nm^{-1}. But for a reflection of 10 nm^{-1} the delocalisation is still very large at a defocus of -70 nm and the minimum delocalisation occurs at a defocus of about -270 nm. No defocus can be chosen to have the minimum delocalisation for all diffracted beams.

In contrast to the HREM images, in which the information is delocalised, the exit wave shows a sharp edge of the specimen and the difference in Debye Waller factor is also clearly seen. Obviously

the exit wave leads to a much more accurate description of the atom positions at and near the surface. Note that the effect of a larger Debye Waller factor is in first approximation quite similar to a smaller scattering potential. In the phase image one can see that the dot corresponding to the Ni atom with the Debye Waller factor of 3 shows a larger extension. Thus, only in combination with the size of the dots a larger Debye Waller factor can be distinguished from a partial occupancy.

2.2. Example 2: reconstructed exit wave of a [100] surface of NiO imaged in profile

Fig. 5 shows a reconstructed exit wave of the (001) surface of NiO in profile and one of the HREM images of the through focus series used for this reconstruction. The black dots in the exit wave correspond with Ni columns in the viewing direction. The Ni atoms are imaged as black dots in the amplitude, whereas the black dots in the phase image correspond to the Ni positions in the thin part of the crystal and to O positions in the thicker part. The black dots of the Ni columns in the amplitude at the
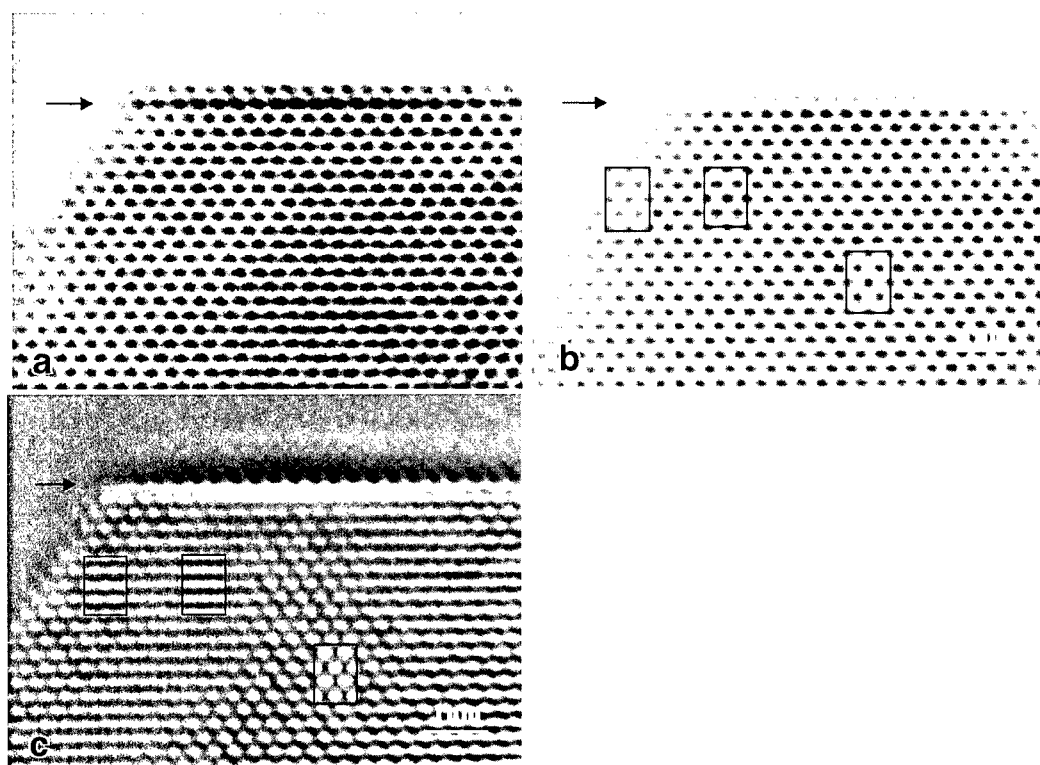
Fig. 5. Profile images of the (001) surface of NiO. (a) Shows an experimental image taken at −100 nm; (b) and (c) shows the amplitude and phase of the exit wave, calculated from a through focus series of 15 images, of which the image (a) is the first image. The dark dots correspond with Ni columns in the viewing direction. The Ni atoms are imaged as dark dots in the amplitude, whereas in the phase image the dark dots correspond to the Ni positions in the thin part of the crystal and to O positions in the thicker part. The black dots of the Ni columns in the amplitude at the surface are less dark, probably due to a larger Debye–Waller factor. The arrows point to the same line position, from which is clear that in (a) one row of black dots is actually located above the surface.

surface are less black, which is probably due to the larger Debye Waller factor, which is normally larger for atoms at the surface. The experimental image does not show this feature of less contrast at the surface because of delocalisation and because it contains information from both the amplitude and the phase of the exit wave (the phase is less sensitive to differences in Debye Waller factors). Furthermore, the experimental image shows one extra row of black dots, situated outside the crystal, which is obviously due to the delocalisation discussed in Example 1.

In case one is only interested in the atomic positions in a single crystalline area, and the crystal is well aligned, a small deviation from the absolute focus will in most cases not lead to a change in the positions of the black or white dots. Thus the atom positions can still be determined quite accurately.

However, in the case of a defect, grain boundary or crystal surface (in profile view), a slight deviation in focus can lead to substantial shifts in the positions of the black dots, as is evident in Fig. 5, which shows the effect of +10, +5, 0, −5 and −10 nm focus shift from the absolute focus for a reconstructed exit wave of a (100) surface of NiO. The focus shifts of +10 and −10 nm result in shifts of the black dots of −0.02 and +0.02 nm away from the bulk respectively.

2.3. Example 3: MoS$_2$ slabs on γ-Al$_2$O$_3$

MoS$_2$ to which cobalt sulfide or nickel sulfide has been added on an atomic scale (CoMoS and NiMoS catalysts, respectively) is employed on a large scale as catalyst in the hydrotreating of oil. In order to

have a large surface area and to prevent rapid sintering to larger particles, frequently γ-Al_2O_3 consisting of small particles is used as support for the CoMoS and NiMoS catalytic phase. MoS_2 is present as slabs, as shown in Fig. 7. The most active phase is believed [30] to be the one for which the edges of the MoS_2 slabs are decorated with Co or Ni (see Fig. 7).

Fig. 8 shows the phase and amplitude of a reconstructed exit wave and one of the HREM images, which was used for the reconstruction. A string of dark dots can be seen in the amplitude image, which are the strongly scattering atoms, e.g. Mo and Co. The last dark dot of the string is much less dark than the others ones, indicating that in this column much less scattering potential is present. This could be due to a large fraction of Co in this column. However, if the slab has a rather pancake-like shape (see Fig. 7b), the projection of the edges will also result in less scattering potential. Finally, the atoms at the edges could have a larger Debye Waller factor. The sulphur atoms are more visible in the phase of the exit wave. The black dots of the sulphur atoms form with the Mo atoms V shapes, which are typical for the MoS_2 structure along this projection. Note that along the electron beam direction the CoMoS slab will probably also have a

curved shape. Only that part of the curved columns of atoms, which is more or less parallel to the electron beam, has resulted in significant contrast.

2.4. Example 4: correction for the delocalisation at an interface

Single crystalline Al_2O_3 (sapphire) is considered as a very suitable substrate material for microwave applications due to its low dielectric losses, availability of large crystals and relatively low cost. Unfortunately, the high reactivity of sapphire with high temperature superconductor materials prevents direct epitaxial growth of thin films. The problem can be solved by the deposition of an intermediate buffer layer. Cubic CeO_2 demonstrates a low reactivity and the ability to epitaxy with R–Al_2O_3 ($1\bar{1}02$) and the YBCO phase. Because of this, it is considered to be a good buffer layer material [31,32]. However, the critical properties of the superconducting layer are strongly dependent on the single crystalline quality and the smoothness of the buffer layer: a smooth surface and a low density of mismatch dislocations in the buffer layer, facilitate the epitaxy of the HTSC layer with high crystallinity and consequently high T_c and J_c characteristics [33]. In this respect, the accommodation of the lattice mismatches at the
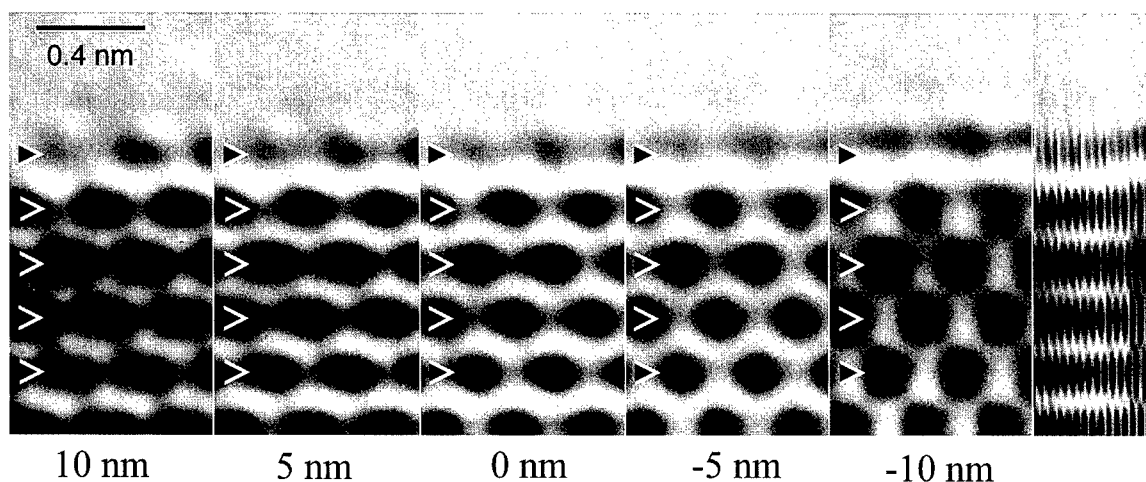

Fig. 6. Experimental exit wave (amplitude) of the (001) surface of NiO in profile view at various focus values. The dark dots correspond with Ni columns in the viewing direction. The applied focus propagations are given below the images. The image on the far right represents the same series of images but compressed in horizontal direction, which is about the same as looking at a glancing angle in horizontal direction. The position of the row of dots at the surface is shifted away from the bulk when a negative focus propagator is applied.
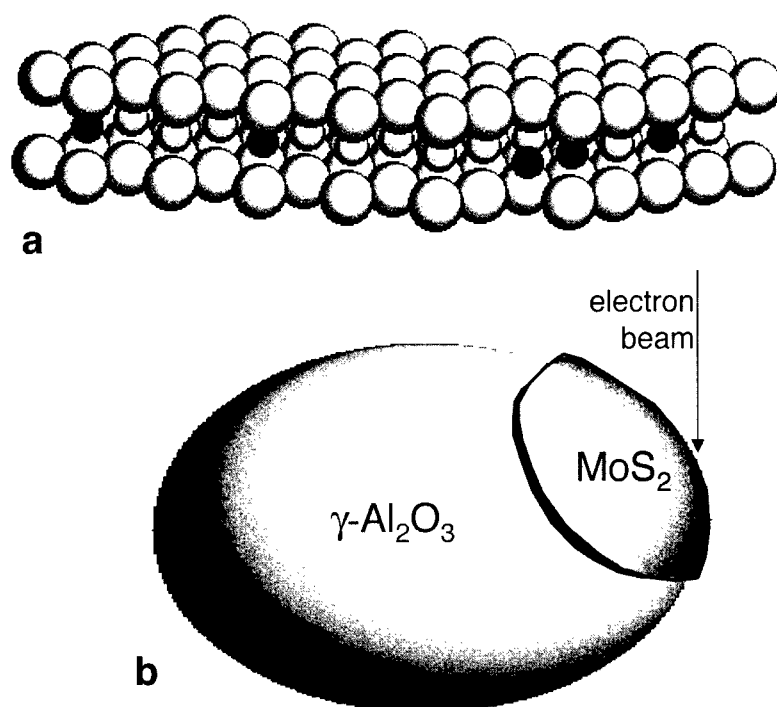
Fig. 7. Schematic representation of the morphology of MoS_2 particles and their location on the $\gamma\text{-}Al_2O_3$ substrate. The position of the Co atoms at the edges is illustrated in (a). The dark small atoms are Co atoms, and the large and small bright atoms are S and Mo, respectively. The covering of the $\gamma\text{-}Al_2O_3$ particle by the MoS_2 particle like a blanket is illustrated in (b).
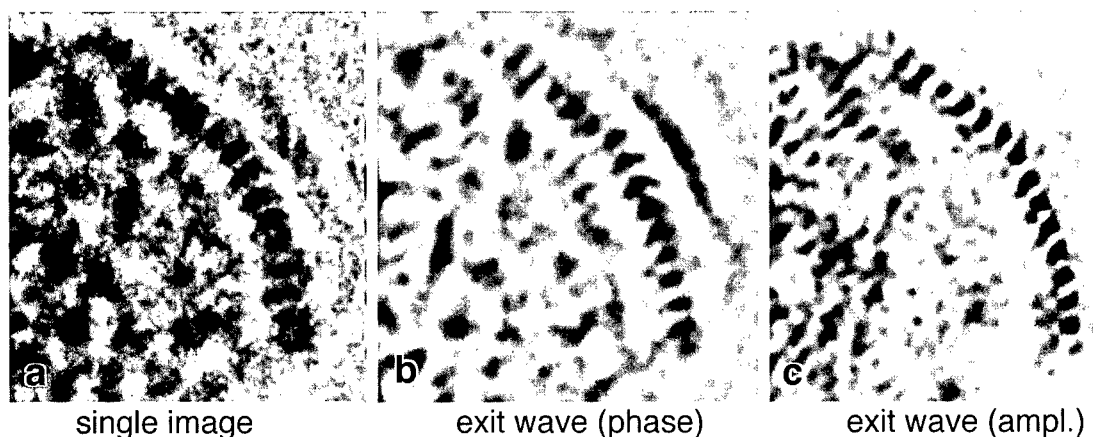

single image   exit wave (phase)   exit wave (ampl.)

Fig. 8. HREM image and exit wave of a MoS_2 particle on $\gamma\text{-}Al_2O_3$. (a) Shows one of the HREM images of the through focus series. (b) and (c) Show the amplitude and phase of the reconstructed exit wave.

$YBCO/CeO_2$ and $CeO_2/R\text{-}Al_2O_3$ interfaces are important for the optimisation of the manufacturing of devices.

Fig. 9 shows images of a sapphire/CeO_2 interface. Fig. 9 show a typical HREM image and a reconstructed exit wave, respectively. Note that, whereas
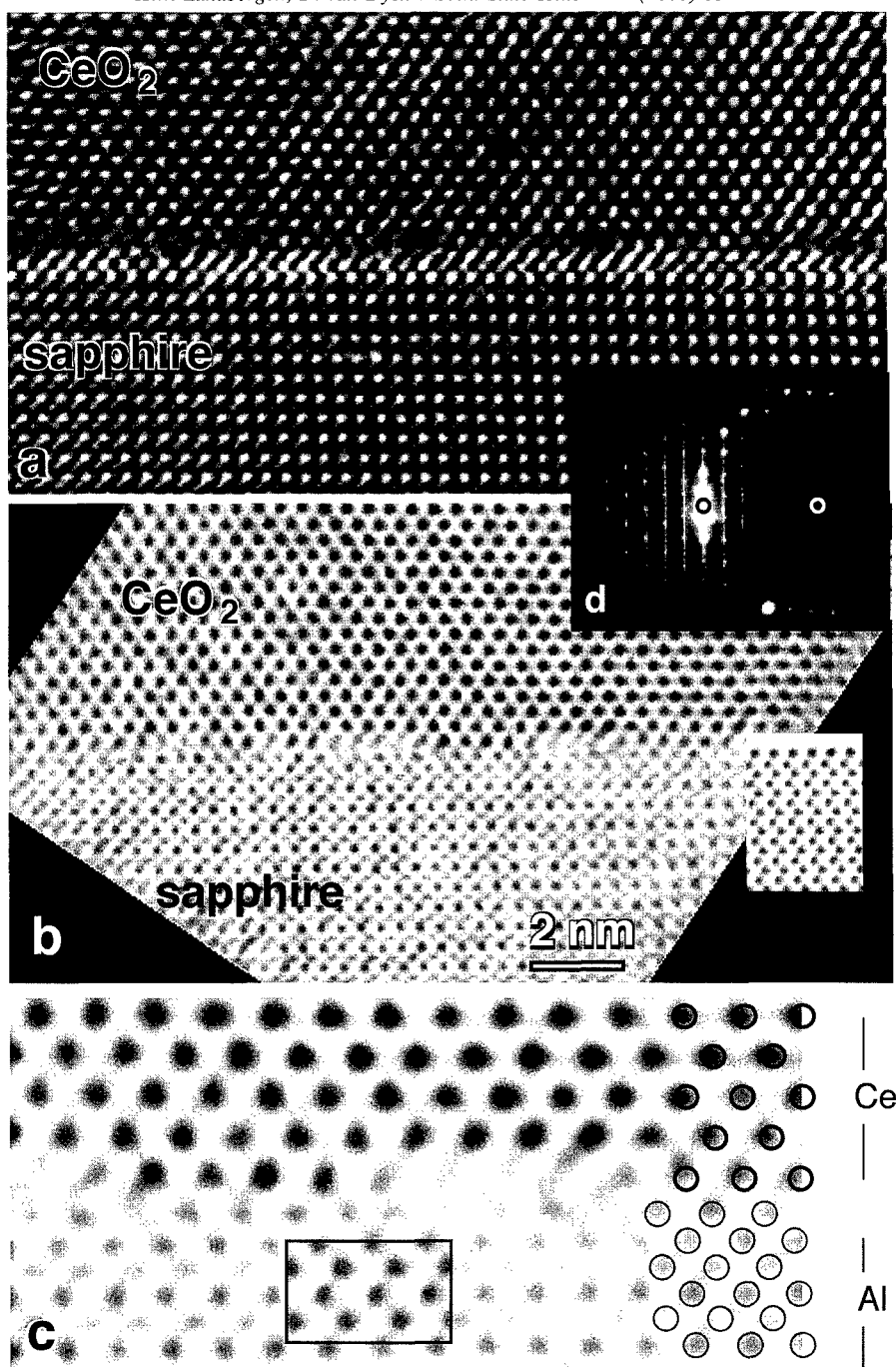
Fig. 9. HREM and exit wave images of the CeO₂/sapphire interface. (a) Shows a HREM image. (b) Shows the amplitude of the reconstructed exit wave. Whereas the exit wave shows a very sharp interface, in the HREM image the interface is fuzzy due to the delocalisation of information. (c) Shows an enlargement of a section of the exit wave. Open circles represent the bulk positions of Ce atoms. The Ce atoms neighbouring the interface are shifted towards the bulk of the CeO_2 layer. (d) Shows a diffraction pattern of an area containing substrate, CeO_2, and YBCO. From this it can be concluded that the sapphire is tilted over 1.7° about the interface normal. Due to the tilt the black dots in the sapphire will not correspond to the Al positions. Insets in (b) and (c) are calculated exit waves using a specimen thickness of 8 nm, a tilt of 1.7° as (d), an isotropic specimen vibration of 0.05 nm, no objective aperture and a defocus spread of 6 nm.

the exit waves reveals a very sharp interface, in the HREM image the interface is fuzzy. This is due to the delocalisation of information occurring in the imaging process. Obviously the exit wave gives much more precise information about the atomic positions at the interface.

The misfit between the sapphire and the CeO_2 lattices, being 5.4% in [10$\bar{1}$1] and 12% in [1$\bar{2}$10] directions, is mainly accommodated in the very first atomic layers of CeO_2, as can be seen in Fig. 9. This figure shows a reconstructed exit wave of the sapphire/CeO_2 interface. At regular intervals one can observe a different contrast in the CeO_2 layer next to the interface. The average spacing between these areas is 4 nm, which agrees well with the dislocation spacing which one expects from lattice parameters mismatch for the (001) lattice spacing of CeO_2 (0.541 nm) and the (1$\bar{1}$02) lattice spacing of sapphire (0.4759 nm). One expects a dislocation spacing of 3.95 nm. The mismatch observable in the image plane should also be present along the viewing direction since in this direction a mismatch also occurs.

An enlargement of the exit wave of the interface is shown in Fig. 9c. The positions of the Ce atoms and the Al atoms, corresponding to their positions in the bulk are given as open circles. The black dots corresponding to the Ce atoms neighbouring the interface are more elongated along the interface normal that the corresponding black dots in the bulk and they are a little bit shifted away from the interface. The elongation might be due to small variations in the positions along the viewing direction. The shift away from the interface suggests an interface relaxation in which the Ce atoms are drawn into the CeO_2 lattice. The black dots at the Ce positions of the first atomic plane of the buffer are absent at the locations of the misfit dislocations. In the phase image of this exit wave, however, one can still observe dots at these sites, which indicates that the atom columns on these sites are less ordered in the viewing direction. This is quite logical given the two-dimensional dislocation network.

The exit wave of the sapphire in Fig. 9c shows two types of dark dots. However, calculated exit waves for sapphire show that these two types of dots are both Al and should have the same intensity, whereby the Al atoms are not in the centre of the

four surrounding Al atoms as is shown in the insets in Fig. 9b and c. In the experimental exit wave the weak dark dots seems to be almost in the centre. This discrepancy can be explained only partly by the rather large misorientation of the sapphire. Image calculations show that for such a tilt the intensities of the two types of dots can be slightly different, but less than in the experimental exit wave. Also the centering of the black dots in the centre of the four surrounding black dots as observed in the experimental image can only be obtained by a shift of the Al position along the c-axis (e.g. z(Al) is 0.372 instead of 0.352). It should be noted that due to the tilt the position of the dark dots in the exit wave would be different from the actual atomic positions. One also has to take into account that when the actual columns of Al atoms are tilted over 1.7°, the projection of the top of the column is shifted over 0.15 nm from the projection of the bottom of the column for an 8 nm thick specimen. Thus although the dark dots corresponding to the Al atoms neighbouring the interface are shifted towards the interface, they might not correspond to the actual position of the Al atoms.

3. Discussion

The electron–matter interaction is sufficiently well understood to allow a calculation of HREM images. Such calculations are frequently used to verify a postulated structural model. In the image simulation algorithm three stages can be distinguished. First, the electron scatters dynamically in the crystal. This interaction can be simulated using the multislice methods. As an input to the multislice program one has to specify all the object parameters such as unit cell, position and type of cell atoms, Debye–Waller factors, object orientation and thickness, and the wavelength of the electrons. The result of this calculation yields the wavefunction at the exit face of the crystal. In a second step, the formation of the image in the electron microscope is simulated where all the instrumental parameters have to be specified. Finally, the electron intensity in the image plane is calculated by squaring the wavefunction. Several commercial software packages [34–37] exist for high-resolution image simulations. For calculations of conventional HREM images one has to do all

three steps. For a calculation to compare with the reconstructed exit wave only the first step with a subsequent band filtering to account for the information limit are required.

Several groups have done excellent quantitative characterisations using HREM images (grain boundaries [1–5], interfaces [38–40] and single-crystalline areas [41]). However, a large majority of the present use of image simulation is that the image comparison is done visually and not quantitatively or in a recursive refinement. Since a large number of parameters can be adjusted, visual comparison is not very reliable. Obviously, a development towards standard use of quantitative comparison is required. A major step in this development is the exit wave reconstruction technique, because that gives more precise data and also forces the electron microscopist to calibrate the microscope and to work according to clear procedures. This is needed because the exit wave can only be correctly interpreted if this is done at the exact focus and with a proper correction of all the lens aberrations, because otherwise phase and amplitude information are mixed. A robust method for determining the exact focus is to exploit the entropy of the exit wave as a function of focus [42,43]. An efficient correction for all microscope parameters is possible with the fingerprint method reported by Thust et al. [44]. The local misorientation can be measured directly by using nanodiffraction. But the change in doses (electrons per unit area) and total electron flux upon switching from nanodiffraction mode to HREM mode can lead to small but very significant changes in the orientation. The determination of the orientation from the exit wave is in principle possible as is illustrated by Bokel et al. [45,46]. They showed that the local misorientation on a unit cell scale could be determined from 'single crystalline' areas in the exit wave, provided this structure is known.

If one wants to determine the structure of an object without modelling a major final step remains: the retrieval of the projected structure of the object from the wavefunction at the exit face. This is certainly not a straightforward process. It is most simple if the object is thin enough to act as a phase object (typically less than 2–4 nm for the compounds discussed in this paper): in that case the phase is proportional to the electrostatic potential of

the structure, projected along the beam direction. However, even in this case it will be very hard or impossible to determine the exact atomic weight of a given dark dot in the exit wave, because its contrast will not only depend on the atoms in the projected column but also on their Debye–Waller factor as is shown in Fig. 2. If the object is thicker, the problem is even more complicated.

However, if the distance between the columns is not too small, a correspondence between the wavefunction at the exit face and the column structure of the crystal is maintained. Within the columns, the electrons oscillate as a function of depth without leaving the column. Hence, the classical picture of electrons traversing the crystal as plane-like waves in the direction of the Bragg beams, which historically stems from X-ray diffraction, is in fact misleading. It is important to note that channelling is not a property of a crystal, but occurs even in an isolated column and is not much affected by the neighbouring columns, provided the columns do not overlap. Hence, the one-to-one relationship is still present in case of defects such as surfaces, interfaces or dislocations provided they are oriented with the atom columns parallel to the incident beam. One can explicitly specify the thickness dependency of the wavefunction at the exit face of a column. In that case the structure can be considered as individual columns of which the scattering and thus the contrast changes with specimen thickness. This leads to a situation that the positions of the black dots in the exit wave do not change their position but do change their relative intensities with thickness. Thus, if the thickness of a specimen is unknown, one is unable to indicate the scattering of a given projected column but the position of this column can be determined quite accurately. In this way the exit wave still retains a strong correspondence with the projected structure, whereby the positions are still (almost) the same but the contrast (in phase or amplitude) cannot be used to determine the scattering potential in the projected structure unless the thickness is accurately known. We used this to determine the structure of $Ce_5Cu_{12}P_9$ [13]; from the exit wave we were able to determine the positions of the columns. This model was the basis of a structure refinement using electron diffraction data for several thicknesses, whereby first the position of the columns was refined assuming all

columns to be equal Cu columns. Next the occupancies were refined, allowing one to decide which atom columns contained, Ce, Cu or P. The final refinement gave very accurate atomic positions.

In conclusion, exit wave reconstruction has now been matured into an important step towards quantitative structure determination of crystalline objects. By extending in this way the resolution limit of the microscope up to the information limit, which is beyond the size of an individual atom, it has become possible to resolve atomic structures without much a priori knowledge. Further development is needed in particular in the interpretation of exit waves from misoriented areas.

Acknowledgements

References

[1] K.L. Merkle (Ed.), Interface Science, Vol. 2, Kluwer, Boston, 1995, pp. 311–345.

[2] G. Möbus, R. Schweinfest, T. Gemming, T. Wagner, M. Rühle, J. Microsc. 190 (1998) 109–130.

[3] W.E. King, G.H. Cambell, S.M. Foiles, D. Cohen, K.M. Hanson, J. Microsc. 190 (1998) 131–143.

[4] O. Kienzle, F. Ernst, G. Möbus, J. Microsc. 190 (1998) 144–158.

[5] G. Möbus, M. Rühle, Ultramicroscopy 56 (1994) 54.

[6] Y. Yan, M.F. Chisholm, G. Duscher, A. Matti, S.J. Pennycook, S.T. Pantelides, Phys. Rev. Lett. 81 (1998) 3675–3678.

[7] D. Van Dyck, H. Lichte, K.D. van der Mast, Ultramicroscopy 64 (1996) 1.

[8] H. Lichte, Ultramicroscopy 47 (1992) 223.

[9] W. Coene, G. Janssen, M. Op De Beeck, D. Van Dyck, Phys. Rev. Lett. 69 (1992) 3743.

[10] P. Peres, F. Weill, C. Delmas, Solid State Ionics 116 (1999) 19–27.

[11] M.R. Palacín, F. Krumeich, P. Gómez-Romero, Solid State Ionics 101–103 (1997) 1079–1085.

[12] K. Kinoshita, J. Bonevich, X. Song, T.D. Tran, Solid State Ionics 86–88 (1996) 1343–1350.

[13] H.W. Zandbergen, J. Jansen, J. Microsc. 190 (1998) 222.

[14] J. Jansen, D. Tang, H.W. Zandbergen, H. Schenk, Acta Crystallogr. A 54 (1998) 91.

[15] S. Nicolopoulos, M. Vallet-Regí, J.M. González-Calbert, Solid State Ionics 101–103 (1997) 175–182.

[16] T. He, C.L. Jia, P. Ehrhart, P. Meuffels, Solid State Ionics 89 (1996) 9–12.

[17] M. Zimnol, A. Graff, H. Sieber, S. Senz, S. Schmidt, R. Mattheis, D. Hesse, Solid State Ionics 101–103 (1997) 667–672.

[18] D. Hesse, Solid State Ionics 95 (1997) 1–15.

[19] J. Walz et al., J. Struct. Biol. 120 (1997) 387–395.

[20] T.S. Bakker, R.H. Cheng, J. Struct. Biol. 116 (1996) 120.

[21] D. Van Dyck, M. op De Beeck, Ultramicroscopy 64 (1996) 99.

[22] D. van Dyck, R.M.J. Bokel, H.W. Zandbergen, Microsc. Microanal. 4 (1998) 428–434.

[23] P. Schiske, in: P. Hawkes (Ed.), Image Processing of Computer-Aided Design in Electron Optics, 1973.

[24] E.J. Kirkland, Improved high resolution image processing of bright field electron micrographs. I. Theory, Ultramicroscopy 15 (1984) 151–172.

[25] W.O. Saxton, Focal series restoration in HREM, in: Proc. XIth Int. Congress on Electron Microscopy, Kyoto, 1986, p. 1, Post deadline contributions.

[26] D. Van Dyck, M. Op de Beeck, in: Proc. XIIth Int. Congress for Electron Microscopy, Seattle, San Francisco Press, San Francisco, 1990, pp. 26–27.

[27] M. Op de Beeck, D. Van Dyck, W. Coene, in: A. Tonomura et al. (Eds.), Electron Holography, North Holland-Elsevier, Amsterdam, 1995, pp. 307–316, ISBN 0-444-82051-5.

[28] F. Phillipp, Mater. Trans. J. Inst. Metall. 39 (1998) 888–902.

[29] K. Mitsuiski, M. Kawasaki, M. Takegushi, M. Furuya, Phys. Rev. Lett. 82 (1999) 3082–3084.

[30] H. Topsoe, B.S. Clausen, E.E. Massoth, in: J.R. Andersson, M. Boudart (Eds.), Catalysis, Science and Technology, Vol. 11, Springer, Berlin, 1996.

[31] F. Wang, R. Woerdenweber, Thin Solid Films 227 (1993) 200.

[32] H.W. Zandbergen, I.E. Graboy, V.L. Svetchnikov, A. Kaul, Physica C (1998) submitted.

[33] I.E. Graboy, N.V. Markov, V.V. Maleev, A.R. Kaul, S.N. Polyakov, V.L. Svetchnikov, H.W. Zandbergen, K.H. Dahmen, J. Alloys Compd. 251 (1997) 318.

[34] P.A. Stadelman, Ultramicroscopy 21 (1987) 131–146.

[35] R. Kilaas, R. Gronsky, Ultramicroscopy 11 (1982) 289–298.

[36] D. Van Dyck, W. Coene, Ultramicroscopy 15 (1984) 29.

[37] D. Van Dyck, W. Coene, Ultramicroscopy 15 (1984) 41.

[38] P. Schwander, W.R. Rau, A. Ourmazd, J. Microsc. 190 (1998) 171–183.

[39] R. Hillebrand, J. Microsc. 190 (1998) 61–72.

[40] V. Radmilovic, S. Ratkovic, U. Dahmen, Microsc. Microanal. 3 (Suppl. 2) (1998) 665–666.

[41] T. Gemming, G. Möbus, M. Exner, F. Ernst, M. Rühle, J. Microsc. 190 (1998) 89–98.

[42] D. Tang, H.W. Zandbergen, J. Jansen, M. Op de Beeck, D. van Dyck, Ultramicroscopy 64 (1996) 265–276.

[43] D. Van Dyck, M. Op de Beeck, D. Tang, J. Jansen, H.W. Zandbergen, in: IEEE Int. Conf. on Image Processing, Los Alamitos, 1996, pp. 737–770.

[44] A. Thust, M.F.H. Overwijk, W.M.J. Coene, M. Lentzen, Ultramicroscopy 64 (1996) 249.

[45] R.M.J. Bokel, J. Jansen, H.W. Zandbergen, Ultramicroscopy 2000 (submitted).

[46] R.M.J. Bokel, J. Jansen, H.W. Zandbergen, D. Van Dyck, in: Proc. 14th Int. Congress on Electron Microscopy, Cancun, Mexico, Vol. II, 1998, p. 407.